GEOFLUIDS

Geofluids (2016) **16**, 43–55 doi: 10.1111/gfl.12135

Permeability evolution in sorbing media: analogies between organic-rich shale and coal

H. KUMAR[1,2,*], D. ELSWORTH[1], J.P. MATHEWS[1] AND C. MARONE[3]

[1]*John and Willie Leone Department of Energy and Mineral Engineering, EMS Energy Institute and G3 Center, Pennsylvania State University, University Park, PA, USA;* [2]*Chevron-ETC, Houston, TX, USA;* [3]*Department of GeoSciences, Pennsylvania State University, University Park, PA, USA*

ABSTRACT

Shale gas reservoirs like coalbed methane (CBM) reservoirs are promising targets for geological sequestration of carbon dioxide (CO_2). However, the evolution of permeability in shale reservoirs on injection of CO_2 is poorly understood unlike CBM reservoirs. In this study, we report measurements of permeability evolution in shales infiltrated separately by nonsorbing (He) and sorbing (CO_2) gases under varying gas pressures and confining stresses. Experiments are completed on Pennsylvanian shales containing both natural and artificial fractures under nonpropped and propped conditions. We use the models for permeability evolution in coal (*Journal of Petroleum Science and Engineering*, Under Revision) to codify the permeability evolution observed in the shale samples. It is observed that for a naturally fractured shale, the He permeability increases by approximately 15% as effective stress is reduced by increasing the gas pressure from 1 MPa to 6 MPa at constant confining stress of 10 MPa. Conversely, the CO_2 permeability reduces by a factor of two under similar conditions. A second core is split with a fine saw to create a smooth artificial fracture and the permeabilities are measured for both nonpropped and propped fractures. The He permeability of a propped artificial fracture is approximately 2- to 3fold that of the nonpropped fracture. The He permeability increases with gas pressure under constant confining stress for both nonpropped and propped cases. However, the CO_2 permeability of the propped fracture decreases by between one-half to one-third as the gas pressure increases from 1 to 4 MPa at constant confining stress. Interestingly, the CO_2 permeability of nonpropped fracture increases with gas pressure at constant confining stress. The permeability evolution of nonpropped and propped artificial fractures in shale is found to be similar to those observed in coals but the extent of permeability reduction by swelling is much lower in shale due to its lower organic content. Optical profilometry is used to quantify the surface roughness. The changes in surface roughness indicate significant influence of proppant indentation on fracture surface in the shale sample. The trends of permeability evolution on injection of CO_2 in coals and shales are found analogous; therefore, the permeability evolution models previously developed for coals are adopted to explain the permeability evolution in shales.

Key words: fracture, modeling, permeability evolution, proppant, shale

Received 22 October 2014; accepted 4 March 2015

Corresponding author: Hemant Kumar, John and Willie Leone Department of Energy and Mineral Engineering, EMS Energy Institute and G3 Center, Pennsylvania State University, University Park, PA 16802, USA.
E-mail: Hemant.Kumar@Chevron.com. Tel.: 832-854-4234. Fax: 8328544234.
*Present address: Chevron-Energy Technology Company, 1500, Louisiana St., Houston, TX 77002 USA.

Geofluids (2016) **16**, 43–55

INTRODUCTION

Carbon dioxide injection in coal seams or shales may be an option for its geological sequestration (Nuttall *et al.* 2005; White *et al.* 2005; Kang *et al.* 2011). The matured shales and coals have similarities in their organic matter content, pore size distribution, and stress regime (Pellenq *et al.* 2012). The porosity and permeability of shale reservoirs are comparable to coalbed reservoirs (Soeder 1988; Shi & Durucan 2010). Shale formations with potential for economical natural gas production such as Marcellus shale (Agbaji *et al.* 2009) contain significant organic matter that may be as high as 10% on a w/w basis (Jenkins & Boyer II 2008; Bruner & Smosna 2011; Kang *et al.* 2011). There are four major types of porous media present in shale: the nonorganic matrix, the organic matrix, any natural frac-

tures, and any hydraulically induced fracture (Wang & Reed 2009). The nonorganic portion is comprised of clay, minerals, and heavy metals (Loucks *et al.* 2009). The organic matrix consists of carbon-rich matter as in the case of coal. It is the presence of organic matter which imparts similar response in both coals and shales upon exposure to sorbing gases (Elsworth *et al.* 2011). Thus, the extensive understanding of coal behaviors and its modeling may be utilized as an analog to model permeability evolution in shales.

A significant portion of sorbing gas is stored in the adsorbed state in bituminous coalbed reservoirs (Laubach *et al.* 1998). Likewise, the organic matter present in shales provides storage capacity for sorbing gas in the organic pores (Wang & Reed 2009). The mass of methane stored as free gas in the fracture porosity is low in shales. However, it is the adsorbed gas in the micropores which contributes to high storage capacity in these rocks (Kang *et al.* 2011). The micropore size distributions (<2 nm) observed in Pennsylvanian coals and Upper Devonian–Mississippian shales are found similar in a recent study (Mastalerz *et al.* 2012).

Physico-sorption/physico-desorption of the sorbing gas in the pores is expected to lead to physico-mechanical changes such as swelling or shrinkage and to correspondingly influence the evolution of permeability in shale reservoirs (Kang *et al.* 2011; Wang *et al.* 2011; Kumar *et al.* 2012) in a manner similar to coal. In both short term and long term, it is the permeability of the fractured porous medium and sorbing media response that controls CO_2 injectivity. Understanding of evolution of permeability is necessary for sequestration management in shale reservoirs. While the transport mechanisms and associated physic-mechanical changes have been studied extensively for coal, few data are available for shales.

Coal permeability is a function of net effective stress (Brace *et al.* 1968; Gash *et al.* 1993) with the permeability decreasing with an increase in effective stress (Somerton *et al.* 1975; Durucan & Edwards 1986; Seidle *et al.* 1992; Bai *et al.* 1995; Min *et al.* 2009). Similarly, the permeability of shale decreases with confining stress which may be attributed to the closure of microcracks (Dong *et al.* 2010). The desorption/adsorption response to gas infiltration also influences permeability evolution (Harpalani & Chen 1995; Seidle & Huitt 1995; Cui *et al.* 2007; Bustin *et al.* 2008; Kelemen & Kwiatek 2009). Coal swells with the adsorption of CO_2 and develops compaction stresses if mechanically constrained (Reucroft & Patel 1986; Siemons & Busch 2007; Day *et al.* 2010; Pone *et al.* 2010). The reduction of coal permeability is thus a consequence of swelling strain with CO_2 sorption (van Bergen *et al.* 2006; Durucan & Shi 2009; Kiyama *et al.* 2011).

The change in gas pressure of a sorbing gas will induce swelling/shrinkage in the organic matrix of shale (Kang *et al.* 2011). For shales, the swelling strain developed by a unit change in gas pressure is expected to be lower than that for coal due to the lower (approximately 10% w/w) organic matter content in shale (Bruner & Smosna 2011). Permeability evolution in shale is also complicated by complex geomechanical processes such as the transport of gas, adsorption, desorption, changing horizontal stresses, and vertical strains. Adsorption of CO_2 in the micropores will result in matrix swelling therefore potentially closing the existing natural fractures and reducing injectivity (Sakhaee-Pour & Bryant 2012). These dynamic changes in shale permeability are fundamentally similar to those for coal (Kumar *et al.* 2010; Mastalerz *et al.* 2012). However, the increase in deviatoric stress beyond a threshold may lead to deformation bands in shale (Dong *et al.* 2010) which is rarely observed in coals. The rearrangement of grains in the deformation bands can lead to the irreversible loss of porosity and concomitant reduction in permeability (Kumar *et al.* 2010). Such observations of permeability reduction beyond a threshold deviatoric stress indicate that the shale may exhibit stress path-dependent permeability evolution (Perez *et al.* 2010).

Conceptual models for transport of sorbing gas in shale have been proposed (Fathi & Akkutlu 2009; Kang *et al.* 2011). The injected CO_2 travels through the open fracture (natural and artificially induced) to the shale matrix. The concentration gradient drives the gas through the inorganic or organic matrix and reaches the organic matter where it is adsorbed and therefore remains stored in the pores. The transport of gas in the inorganic matrix may result from transitional-slippage or diffusion-related mechanisms or a combination of both (Kang *et al.* 2011). The effect of mineral heterogeneity may also be coupled with conceptual models to predict the effect of macrokinetics and macrotransport on the potential reduction of ultimate recovery (Fathi & Akkutlu 2009). Primary methane recovery remains poor without stimulating the shale gas reservoir. Therefore, shale gas reservoirs are often fractured using water slurry and cross-linked gels to develop a network of artificial fractures to enhance the permeability of the pay zone (Veatch *et al.* 1989; Arthur *et al.* 2008; Boyer & Kieschniek 2010). Enhanced gas recovery from shale reservoirs may also be achieved by injecting CO_2 (Nuttall 2010) but it may further accelerate the fracture closure by inducing swelling in the organic matter of shale (Curtis 2002), a phenomenon which is commonly observed in coal (Harpalani & Schraufnagel 1990; Harpalani & Chen 1995; White *et al.* 2005; Wang *et al.* 2011; Kumar *et al.* 2014). However, evolution of permeability in proppant-filled fractures under the application of stress and sorption-induced swelling caused by CO_2 has not previously been evaluated. In this work, we have answered the following questions: (i) How does permeability evolve in a nonpropped and propped artificial shale fracture upon injection of He and CO_2? (ii) What is the role of confining stress and sorptive

gas pore pressure on permeability evolution in shale? (iii) How does proppant indentation affect the fracture roughness under the influence of sorptive gas? (iv) Are the permeability evolution trends in shale similar to the trends observed for coal? (v) Does the proposed mechanistic model fit the experimental observations?

EXPERIMENTAL METHODS

Forced fluid-injection experiments were completed on a cylindrical core, axially saw-cut, then propped or non-propped with # 70–140 proppant. These samples were stressed to *in situ* conditions. He and CO_2 were used as permeants to investigate the role of swelling and effective stress on the dynamic evolution of permeability.

Samples

The two cylindrical cores of shale, 2.5 cm diameter and 5 cm length, were sampled (drilled along bedding) from shale blocks collected in Pennsylvania (Fig. 1A). Shale density varied between 0.95 (named as sample 'A') and 1.58 gm cm^{-3} (named as sample 'B') between the two sampled locations. The He porosity of the low-density shale (A) was 34%, while the high-density sample (B) was 5% as determined using the pulse test technique. The fixed carbon, ash yield, and moisture contents were 8%, 87%, 1% for sample A and 5%, 92%, 0.5% for sample B (ASTM International D7582 2010). It should be noted here that these samples are not fully representative of commercially producing shales in Pennsylvania.

The evolution of permeability was investigated by injecting He and CO_2 into an intact shale core. Shale gas reservoirs are typically fractured to enhance the permeability, and proppants are concurrently placed into the fracture to retain the enhanced permeability. Here, an artificially saw-cut fractured core was prepared to evaluate the role of the fracture on permeability evolution. The fractured core was permeated using He and CO_2. Cores were cut in half (axially) using a thin diamond-coated blade to produce smooth opposing surfaces forming an idealized fracture (Fig. 1B). A uniform monolayer of # 70–140 proppant sand was sandwiched between the fracture surfaces to test the influence of propped fractures on permeability evolution (Fig. 1C). The cores were wrapped in aluminum foil to prevent any adsorption or diffusion of CO_2 through the rubber jacket during the permeability experiments. Surface roughness was quantified by optical profilometry both pre- and postexperimental sequences (Kumar *et al.* 2009; Rousseau *et al.* 2010).

Apparatus

A simple triaxial apparatus was used for the injection of various gases under predefined effective stress paths and the permeability measured concurrently (Fig. 2). All experiments were completed in constant stress mode. The apparatus comprised a triaxial cell to confine the sample at prescribed stresses, an axial strain gauge to monitor the shrinkage or swelling in the axial direction, ISCO syringe pumps to apply stresses and to measure volume strains (axial and confining), pressure transducers to monitor the upstream and downstream reservoir pressures and a data acquisition system. Additional details of the equipment are described elsewhere (Kumar *et al.* 2012). The transient pulse test method was used to determine the permeability of the samples. The permeability was evaluated from the rate of pressure decay/gain in the upstream/downstream reservoirs (Brace *et al.* 1968) assuming that there was no sorption during the short-duration (<10 min) experiments.

Procedures

The shale cores were placed within the triaxial core holder and predefined stresses were applied. The experiments were conducted at a constant confining stress of 10 MPa

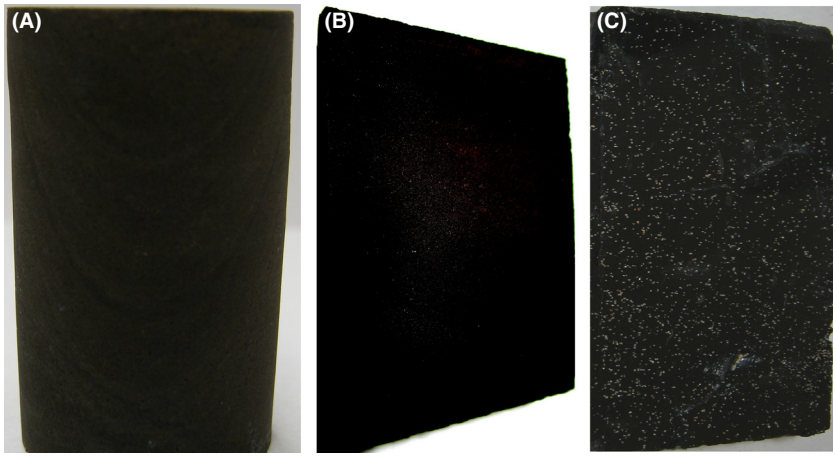

Fig. 1. (A) A cylindrical shale core used in the experiments. (B) The fracture surface of the saw-cut split shale core. (C) The fracture surface with monolayer of #70–140 proppant on it. This image has been enhanced electronically to achieve higher contrast.

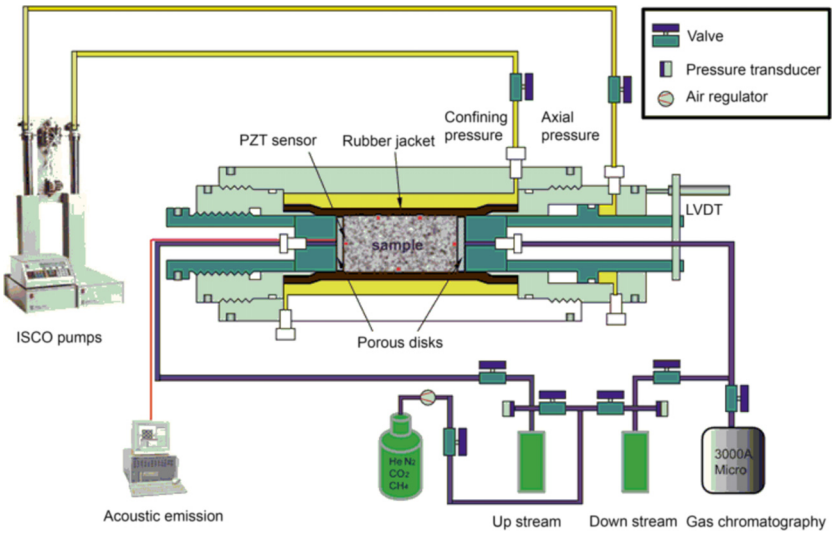

Fig. 2. Schematic of a typical transient pulse test permeability apparatus (Wang *et al.* 2011).

(equivalent to an effective stress at approximately 1000 m or approximately 3500 feet depth). The respective roles of confining stress, deviatoric stress, and sorption on the evolution permeability were explored using intact cores. The experiments consisted of sequential injection of He and CO_2. Also, a suite of experiments was conducted on saw-cut shale core, absent proppant, to explore the permeability evolution of an artificial fracture in response to injection of both inert (He) and sorbing (CO_2) gases. Table 1 provides the ranges of experimental variables and measured outputs.

The following experimental sequence was followed for a shale sample containing a single artificial fracture under constant isotropic stress with incremental gas pressures:

(1) *Nonpropped fracture He permeability*: Helium was circulated in nonpropped shale sample.
(2) *Nonpropped fracture CO_2 permeability*: The sample was permeated with CO_2 and permeability was measured by pulse test at different saturated conditions (gas pressures 1–6 MPa).
(3) *Propped fracture He permeability*: The artificial fracture was propped with a monolayer of #70–140 sand. Helium was injected and the permeability was measured.
(4) *Propped fracture CO_2 permeability*: The sample was vented and permeated using CO_2. The permeability was measured on the CO_2-saturated sample.

We have chosen to complete these experiments using CO_2 to understand the limiting case of swelling and embedment in shales. Pre- and postexperiment surface micrographs were captured using optical interferometry. The micrographs contain surface roughness information including the peak-to-pit height differential with high fidelity (resolution 1 μm). The surface micrograph was obtained pre- and postexperiments for a selected surface area measuring 2.3 by 1.7 mm. The same core was utilized for both pre- and postexperiment optical measurements. It is important to note that an intact sample was used to explore the permeability evolution and then it was artificially fractured to explore permeability evolution in the presence of this artificial fracture. The injection experiments were repeated with the proppant-filled artificial fracture. Details of the optical profilometry may be found elsewhere (Kumar *et al.* 2009).

Table 1 Suite of variables and prescribed ranges utilized in the experiments, for gas pressure P_p, permeability k, axial stress σ_1, confining stress σ_3, and axial strain σ_a.

Experimental variables	Experimental range	Measured outputs
Temperature	Constant	N/A
Gas pressure	1–6 MPa	P_p
Axial stress σ_1	10, 15, 20 MPa	σ_1
		σ_3
		ε_a
Confining stress σ_3	10, 15, 20 MPa	
Gas type	He, CO_2	N/A

Data processing methods

The transient pulse test method was utilized to evaluate shale permeability (Brace *et al.* 1968). In a typical run, a shale core was packed and placed under axial and radial stress in the triaxial apparatus as shown in Fig. 2. A mild vacuum (approximately 25 mm Hg) was applied to evacuate the air from the combined sample and reservoir system. The core was saturated with gas (He or CO_2) to an equilibrium pressure before applying a pressure pulse. A pressure pulse was allowed to flow through the core from the upstream reservoir to the downstream reservoir until the pressure reached equilibrium, that is, upstream and downstream pressures were approximately equal. The applied pressure pulse was significantly smaller (<10%) than the initial gas pressure in

the system – to avoid significantly altering effective stresses. We have assumed that there was insignificant additional adsorption with less than a 10% increment in gas pressure. The pressure loss in the upstream reservoir and pressure gain in the downstream reservoir were recorded with time. This process was repeated until the predetermined value of gas pressure was achieved. The pressure–time profile from the experiment was used to obtain permeability, k from Eq. 1 (Brace *et al.* 1968).

$$k = \frac{\gamma \cdot \mu \cdot L \cdot V_{up} V_{down}}{P_{eq} \cdot A \cdot (V_{up} + V_{down})} \quad (1)$$

where permeability k (m^2) is calculated from the decay parameter γ (sec^{-1}) for a known gas viscosity μ (Pa.s), sample length L (m), equilibrium pressure at the end of the experiment P_{eq} (N m^{-2}), and cross-sectional area of the specimen A (m^2) relative to upstream/downstream reservoir volumes $V_{up/down}$ (m^3), measured initial pressure $p_{up/down^0}$ (N m^{-2}), and transient upstream/downstream reservoir pressures $p_{up/down}$ (N m^{-2}). The value of γ is the slope of the line obtained from a $\log\left(\frac{d(p_{up}-p_{down})}{(p_{up^0}-p_{down^0})}\right)$ versus time straight line plot from Eq. 2. This method yields a single value of permeability for a single pulse.

$$\gamma = \frac{\log\left(\frac{d(p_{up}-p_{down})}{(p_{up^0}-p_{down^0})}\right)_t}{dt} \quad (2)$$

Pressure decay in the upstream reservoir and complementary pressure gain in the downstream reservoir for a typical pulse test with a nonadsorbing (He) gas are shown in Fig. 3. Pulse-decay data were reduced for $dP_0 = p_{up^0} - p_{down^0}$, $dP_t = p_{up} - p_{down}$ and P_{eq}. A typical set of observations was used for the calculation of percentage error in the permeability. Further details of the analysis and error propagation may be found elsewhere (Kumar *et al.* 2012).

Gas slippage as quantified in the Klinkenberg effect is typically observed when the dimensions of flow channels are comparable to the mean free path of gas molecules causing the gas molecules to slip on the rock surface (Klinkenberg 1941; Amyx *et al.* 1960). The observed reduction in permeability with increasing injection pressure at a constant confining stress may be attributed to slippage factor if the permeating media does not swell on exposure to the injected gas (Zhu *et al.* 2007; Kumar *et al.* 2012). The Klinkenberg slippage factor is a function of gas molecule slippage along the pore walls at low values of pore pressure (Rahmanian *et al.* 2010). We eliminated the possibility of the Klinkenberg effect as the size of the pores in the intact core was significantly larger than the mean free path of the gases (He and CO_2).

RESULTS

The parametric evaluation of permeability evolution was completed for shale. Permeability experiments in shale for both He and CO_2 were carried out by injecting the gases under constant total stress of 10 MPa into intact and fractured shale cores while the gas pressures were varied within a range as given in Table 1. The following sections report observations and investigate the role of confining stress, deviatoric stress and sorption on permeability evolution in intact shale core, shale core containing artificial fracture, and shale core containing propped artificial fracture.

Confining stress

The shale core was permeated with He and gas pressures incremented under constant isostatic stresses of 10, 15, and 20 MPa to measure the permeability. The confining stress was increased in steps by the injection of fluid into the triaxial cell (Fig. 2). Shale permeability may vary with transitions in stress pathways (Dong *et al.* 2010). The axial and confining stresses were increased simultaneously and at the same rate in an effort to retain deviatoric stress rela-

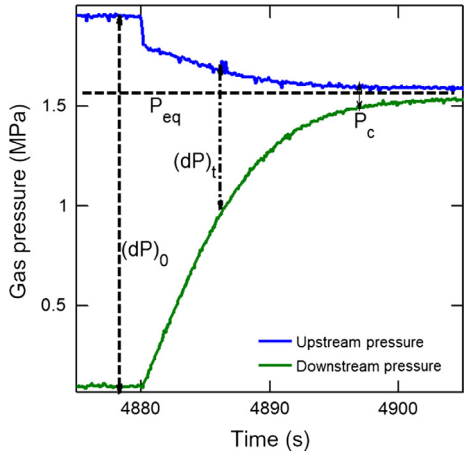

Fig. 3. A typical transient pulse test response taken from (Kumar *et al.* 2012).

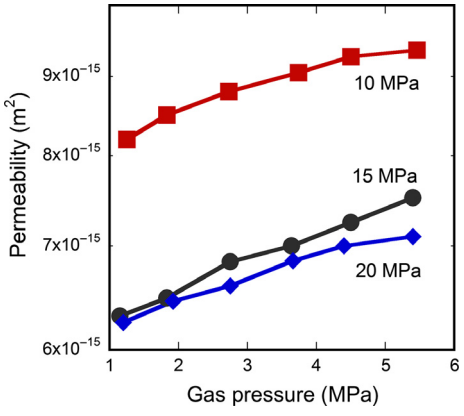

Fig. 4. Permeability evolution of intact shale sample A upon injection of He at constant confining stresses of 10 MPa, 15 MPa, and 20 MPa.

tively constant during loading. The permeability increased with gas pressure at all constant confining stresses (Fig. 4). This is consistent with the opening of microfractures as effective stress decreases in an intact shale core. For example, the increase in permeability was approximately 15% as the gas pressure was increased from 1 to 6 MPa at a constant confining stress of 10 MPa. Similar observations were made at higher confining stresses of 15 and 20 MPa (Fig. 4). These observations were consistent with shale permeability evolution data reported by others (Soeder 1988; Dong *et al.* 2010; Cho *et al.* 2012).

Sorptive gas injection

The role of gas sorption on shale permeability evolution was investigated by injecting CO_2 into the intact core at constant confining stress of 10 MPa (Fig. 5). A reduction in permeability was observed with an increase in gas pressure for both low-density (sample A) and high-density (sample B) shale. The permeability at 1 MPa was approximately double the minimum permeability observed at approximately 4 MPa in sample A. However, the permeability reduction in sample B was relatively small (approximately 20%) with a change in gas pressure from 1 to 4 MPa. It is notable that the magnitudes of permeability reduction were different for two samples which may be attributed to their compositional (organic matter, clay, heavy minerals) and lithologic differences.

This permeability reduction was the result of the dominant swelling response of the organic component of the organic-rich shale relative to the dilation of natural fractures. This occurs for gas pressures below approximately double the Langmuir pressure. At gas pressures above this double-Langmuir threshold, permeability reduction halted and the permeability then increased (Kumar *et al.* 2010). These findings are consistent with observations of permeability evolution concurrent with injection of a sorbing gas (CH_4) in a gas shale sample collected from Alberta, Canada (Letham 2011). Similar behavior is also reported for various coals upon injection of CH_4 and CO_2 (Pini *et al.* 2009; Kumar *et al.* 2012; Wang *et al.* 2012). The permeability of the low-density sample was one hundred times larger than that of the high-density shale sample. However, the behavior exhibited by both samples upon injection of CO_2 was similar (Fig. 5). The sample was evacuated using a mild vacuum at the completion of the CO_2 permeability test, and He was injected to evaluate the post-CO_2 flow permeability of the core. The He permeability after the CO_2 flow was a fraction of the original He permeability (not shown). The He permeability partly recovered as the desorption of CO_2 continued with He injection. These observations are analogous to the permeability evolution in bituminous coal (Kumar *et al.* 2012).

Nonpropped and propped artificial fracture

The shale sample with an artificial fracture was permeated with He and CO_2, and the permeability evolution was determined for the idealized nonpropped and propped fractures. Sample 'A' was chosen for these experiments as it shows significant variation in permeability with gas pressure (Fig. 5). Hence, sample A should provide a conservative data set to estimate the validity of the model developed. A monolayer of the proppant was laid as uniformly as possible on the surface of the shale and the permeability of the propped artificial fracture determined. The permeability evolution was measured at a constant confining stress of 10 MPa with varying gas pressures (Fig. 6). The He permeability of the propped fracture was approximately 2–3 times higher than that of the nonpropped frac-

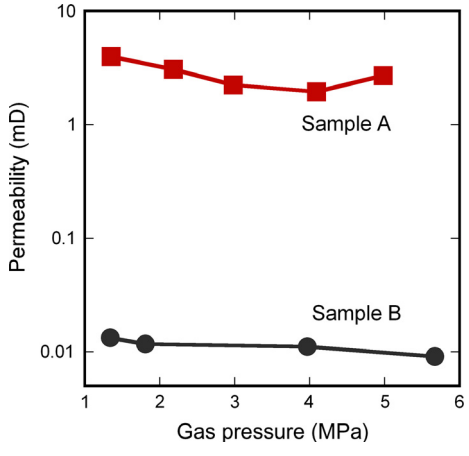

Fig. 5. Permeability evolution in two shale samples (A and B) upon injection of CO_2. The observations were made in the order of incremented gas pressures at a constant confining stress of 10 MPa.

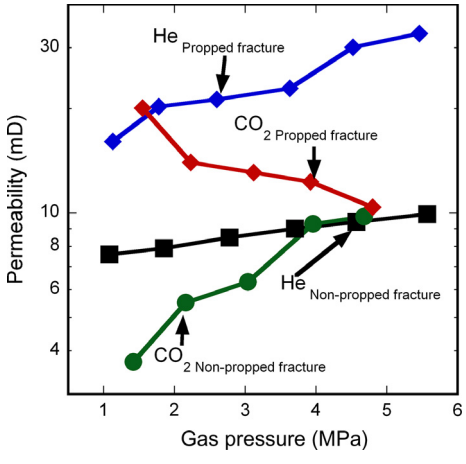

Fig. 6. Permeability evolution in a shale core (saw-cut sample A) with a nonpropped and propped fracture upon injection of He and CO_2. The gas pressure is incremented at a constant confining stress of 10 MPa. The curves are indicated in the figure.

ture (Fig. 6). The permeability of the artificial fracture increased exponentially with decreasing effective stress in both nonpropped and propped cases. The permeability increased by approximately 30% in the nonpropped fracture compared to approximately 100% in the propped fracture with gas pressure increasing from approximately 1 to approximately 5 MPa. The rate of change of permeability with gas pressure was greater in the propped fracture relative to that in nonpropped fracture (Fig. 6). The permeability evolution in nonpropped and propped artificial fractures in bituminous and anthracite coal is known to exhibit similar behavior (Kumar *et al.* 2013).

The CO_2 permeability evolution of nonpropped and propped artificial fractures in shale was next evaluated. The CO_2 permeability of the nonpropped fracture increased with an increase in gas pressure (Fig. 6). The increase in permeability of the propped fracture was as high as approximately 5fold that of the nonpropped fracture depending upon the conditions under which permeability was evaluated. Interestingly, the permeability evolution in the propped fractures exhibited behavior similar to that of intact coal (Kumar *et al.* 2013). The permeability evolution of the propped fracture in shale upon injection of CO_2 is shown in Fig. 6. Although, the permeability evolution for this sample did not show the typical 'U-shaped' response of permeability versus gas pressure (Fig. 6) observed in our other work (not shown here) this is likely specific to this particular sample and under these specific conditions.

DISCUSSIONS

The permeability evolution in the nonpropped and propped shale fracture is orchestrated mainly by confining stress and sorptive gas pressure in the pores. Also, the evolution of permeability in the intact shale sample was found to be dependent on these two factors. There are several models for permeability evolution in coal. These models utilize the change in stress and sorptive gas pressure to predict the permeability evolution. These models may be divided between strain-based, stress-based, and empirical models (Palmer 2009). Here, we adapt a stress-based mechanistic model describing permeability evolution in coal (Kumar *et al.* 2012) to explore permeability evolution in shale upon injection of a sorbing gas. Furthermore, we used a mechanistic model, developed for permeability evolution in propped artificial fractures in coal (Kumar *et al.* 2013) to explain similar permeability observations in artificially fractured shale in the following subsections. Also, we have discussed the implication of organic matter swelling in shales in the last subsection.

Permeability evolution in intact shale core

The evolution of permeability upon injection of CO_2 in various rank of coals is observed to vary with stress, pressure, and moisture content (Kumar *et al.* 2012). These represent the principal features that impact permeability evolution in swelling media (e.g., Eq. 3).

$$\frac{k}{k_0} = \left\{ \left(1 + \frac{\text{c.p}}{p + P_L} \right)^3 + \text{e}^{-\beta\sigma'} \right\} * \text{e}^{-\delta S_w} \tag{3}$$

where permeability k, initial permeability k_0, gas pressure p, Langmuir pressure P_L, and assumed fitting constant C, effective stress σ', moisture content S_w, and scaling parameters β and δ define the response. The scaling parameter C is defined as $C = (\frac{\varepsilon_L S^2}{a b_0})$, where initial fracture aperture b_0, fracture length a, fracture spacing s, and peak Langmuir strain ε_L represent the response. We have applied this mechanistic model to describe permeability observations that result upon injection of CO_2 in the two shale samples (A & B) used for this study. The fitting parameters for C, P_L, β and δ in this model are strain index, Langmuir pressure, stiffness index, and interaction index, respectively. The shale samples used for this study were dry; therefore, the water content ($S_w \cong 0$) is assumed to be zero. This assumption eliminates one parameter (δ) in the model. The remaining parameters (C, P_L, β and δ) are recovered using an optimization against the permeability observations. The details of the optimization may be found elsewhere (Kumar *et al.* 2012).

The normalized permeability evolution data upon injection of CO_2 in intact shale samples (A & B) is shown (Fig. 7). The normalizing factor used for these observations is the base magnitude of He permeability at null confining stress, that is, k_0. The values of k_0 were 1.09×10^{-14} m^2 and 3.16×10^{-17} m^2 for samples A and B, respectively. The goodness of fit was 92.1% and 86.6% for sample A and B indicating that the trend predicted by the proposed model demonstrated acceptable fits to the experimental values (Fig. 7). The values of the fitting parameters are shown in Table 2. The absence of CO_2

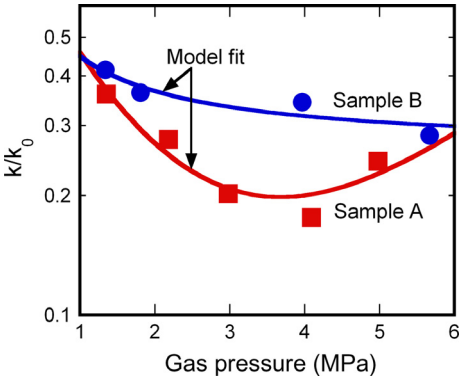

Fig. 7. Analytical fits to the mechanistic model for the observations of permeability evolution upon injection of CO_2 in the two intact shale samples. The low-pressure portion (<3.5 MPa) of the curve is dominated by swelling response, while the high-pressure portion (>3.5 MPa) is dominated by dilation promoted by diminishing effective stresses.

Table 2 Typical value of the fit parameters. See text for the definition of fit parameters.

	Fit parameters		
Sample	C	P_L	β
A	1.02	3.00	0.34
B	0.36	0.53	4.99

adsorption and swelling-induced strain measurement data on Pennsylvanian shale restrict us from any direct parametric comparison. However, we present the congruence of fitting parameters below.

(1) *Parameter C:* The Langmuir strain may be expressed as $\varepsilon_L = \frac{Cab_0}{S^2}$. The larger values of C indicate higher values of maximum swelling-induced strain (ε_L). The swelling-induced strain in sample A (lower density shale) was approximately 3fold that of sample B (higher density shale) if other parameters (a, b_0, and s) were assumed to be same for the two samples. This may be attributed to the higher organic matter content of sample A as compared to sample B.

(2) *Parameter P_L:* Langmuir pressures P_L for samples A and B were 3.0 and 0.5 MPa, respectively. Minimum permeability occurs at approximately 3.5 MPa for sample A, while sample B did not show a point of inflexion in the observed gas pressure range.

(3) *Parameter β:* The parameter β for sample B was approximately 10- to 15-fold that of sample A. This indicates that sample B is stiffer than the sample A. Consequently, the permeability of sample B is less affected by changes in effective stresses. These findings are consistent with the permeability observation made above.

It is important to note that the variation in values of the parameters (P_L and ε_L) may yield different production characteristics.

Permeability evolution of propped artificial fracture in shale core

A mechanistic model for permeability evolution in a propped artificial fracture in coal is applied to represent the response in shale. This model assumes that the proppant grains act as 'bridges' that partially embed into the shale matrix (Fig. 8).

Correspondingly, the permeability of a propped artificial fracture is much higher than the shale matrix but also much more sensitive to changes in pressure. This is because the void volume available for flow (CO_2) is modulated with both overburden stress and swelling, with this in turn affecting the permeability. The mechanistic model developed by (Kumar *et al.* 2013) assumes that the permeability modulates as a function of proppant embedment and sorption-induced swelling. The mathematical formulation of their model is presented below.

The embedded radius of a hard sphere (proppant) pressed against a flat surface (shale fracture surface) can be represented (Bower *et al.* 1993; Mesarovic & Fleck 2000; Jamari & Schipper 2005) (Fig. 9),

$$r_1 = R\sqrt{\frac{\sigma'}{\pi c}} \tag{4}$$

here, r_1 is the radius of the portion (circular) embedded into the surface, R is the radius of proppant grain, σ' is the effective stress, and c is the cohesive strength of shale.

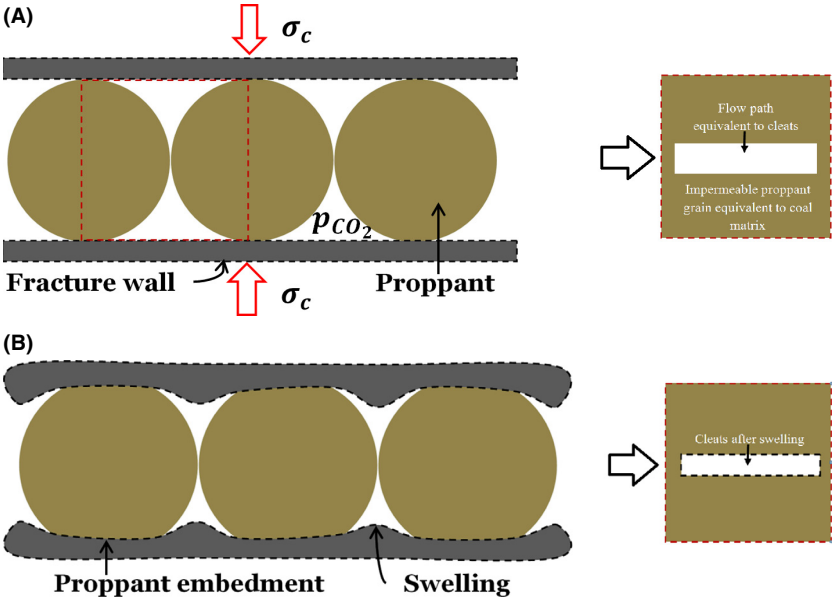

Fig. 8. The sorption-induced swelling and normal stress-driven embedment are shown. A single unit is shown in red dashed lines (A) before the application of normal stress and sorptive gas pressure (B) after proppant embedment and swelling (Kumar *et al.* 2014)

The embedded height (h_1) of sandwiched proppant grain,

$$h_1 = R\left(1 - \sqrt{1 - \frac{\sigma'}{\pi c}}\right) \tag{5}$$

The total volume V_1 of proppant grain embedded into the two fracture surfaces can be calculated as,

$$V_1 = 2\frac{1}{3}\pi h_1^2(3R - h_1) \tag{6}$$

Consider a cubical unit of shale of side $2R$ containing a proppant grain as shown in Fig. 8 with red dashed lines. The volumetric strain developed in this unit due to sorption-induced swelling may be written as,

$$\Delta V = \alpha\varepsilon_L\left(\frac{P}{P + P_L}\right)(2R)^3 \tag{7}$$

here, ΔV is the volumetric strain developed through swelling, α is a arbitrary shape factor, P is the pore pressure of gas, and P_L is the Langmuir pressure. The arbitrary shape factor is an index to measure the local volume of shale affected by sorptive gas injection (Liu *et al.* 2011).

If h_2 is the resultant new embedded height due to stress and swelling then the change in embedded volume can be represented as,

$$2\frac{1}{3}\pi h_2^2(3R - h_2^2) = V_1 + \Delta V \tag{8}$$

$$2\frac{1}{3}\pi h_2^2(3R - h_2^2) = 2\frac{1}{3}\pi h_1^2(3R - h_1) + \alpha\varepsilon_L\left(\frac{P}{P + P_L}\right)(2R)^3 \tag{9}$$

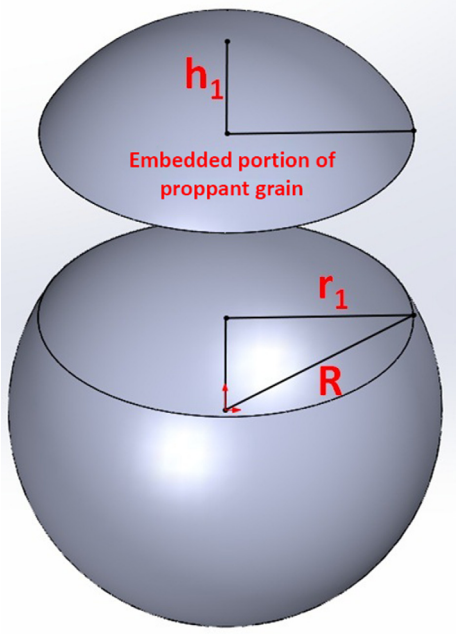

Fig. 9. Three-dimensional cartoon (highly exaggerated) of a proppant grain particle. The top portion shows the embedded part (Kumar *et al.* 2014).

The new embedded height h_2 can be calculated from Eq. 9. The effective aperture of fracture b at any point during varying pore pressure at constant confined stress can be written as,

$$b = 2R - h_2 = b_0 - \Delta b \tag{10}$$

here, b_0 is the initial fracture aperture.

The change in aperture of the fracture Δb driven by these processes may be represented as,

$$\Delta b = -\Delta h_2 \tag{11}$$

For the cases where bulk *in situ* permeability k_0 is known at fracture aperture b_0 then the permeability evolution with change in aperture can be evaluated (Liu *et al.* 1997). This allows the evolution of fracture permeability to be followed for an arbitrary evolution of fracture aperture (Elsworth & Goodman 1986; Piggott & Elsworth 1993). It has been assumed that flow occurs in fractures only. The permeability of fracture k is modulated based on its initial permeability k_0 as follows.

$$\frac{k}{k_0} = \left(1 + \frac{\Delta b}{b_0}\right)^3 \tag{12}$$

The formulation allows the evolution of normalized permeability to be represented with change in fracture aperture. The arbitrary shape factor (α) and cohesive strength (c) of shale are evaluated from the best fit as indexed by the coefficient of correlation (R^2). Here, it is important to note that the change in aperture of the propped fracture Δb would govern the permeability evolution presented in Fig. 6.

This formulation allows the evolution of normalized permeability to be represented with the change in fracture aperture as a combined response to both normal stress and sorptive gas pressure in the fractured core. The arbitrary

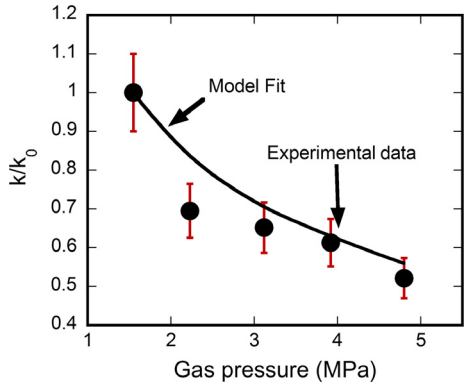

Fig. 10. The evolution of permeability in a propped fracture in shale upon injection of sorbing gas CO_2. Uncertainty in the permeability magnitude is within ±10% as indicated by error bars. The model fit is shown by the solid line.

Table 3 Factors influencing permeability evolution in high organic content and high-swelling materials (e.g., coal) relative those influencing the response of lower organic content shales.

Type	Coal gas	Shale gas
Relative carbon content	High	Low
Free gas content	Low	High
Sorptive strains	High	Low
Fracture network geometry	Small spacing	Large spacing
Comparative permeability	High	Low
Permeability sensitivity to deformation	Low	High
Linkage: permeability-to-sorption	Significant	Significant
Stiffness	Low	High
Strength	Low	High

shape factor (α) and cohesive strength (c) of shale are evaluated from the best fit as indexed by the coefficient of correlation (R^2). As noted in section 4.1, the magnitudes of the Langmuir strain and Langmuir pressure are 1.5% and 4 MPa, respectively. The initial permeability (k_0) and fracture aperture (b_0) are chosen from the first point of observation in the permeability experiments and the MATLAB® curve fit toolbox used to optimize the values of the parameters α and c. Fig. 10 shows the model fit with experimental observations for the coal sample 'A'. The values predicted from curve fitting for α and c are 2 and 10 MPa. Unfortunately, no direct comparison of cohesive strength values can be made due to the absence of any published data for the cohesive strength of these shales; however, the value of c lies within the expected values reported elsewhere (Chen *et al.* 2003).

Interestingly, the significant influence of swelling strains on the evolution of permeability in both unpropped and probed fractures is unanticipated, when considering the low mass percentage of organic material present in shales (<20%) relative to coals (>90%). As sorption-induced changes in permeability result from the swelling strains induced within the organic fraction, their magnitude should scale with the organic fraction. A reduced mass-based fraction of organic material, and hence reduced magnitude of induced strain, may still result in a significant change in permeability if both the initial permeability of the shales low and the initial fracture spacing is high – both in relation to high organic fraction coals – as noted in Table 3. As fracture spacing increases, the scaled swelling displacement resulting from a given uniform strain, but concentrated onto a single fracture (Δb), increases. Thus, the resulting change in permeability that scales as $k/k_0 \sim (1 + \Delta b/b_0)^3$ may still be significant even if the magnitude of the swelling strain (ε_L) is significantly smaller in shale than in coal.

Observations with White Light Optical Profilometry

White light optical profilometry was utilized to quantify and characterize the surface of the shale both pre- and postexperimental sequences. The advanced facility of optical profilometry allowed in capturing a significant portion of the features on the fracture surface even in the absence of good reflective surface. High-magnification three-dimensional surface micrographs (approximately 300) were acquired and stitched together to obtain a micrograph covering a 2.3 × 1.7 mm patch. Surface characteristics were compared both before and after the experimental suite.

Deep and wide interconnected pores were found uniformly distributed on the shale fracture surface (Fig. 11A) indicating relatively higher permeability (~mD) as measured in the experiments (Fig. 4). In the micrographs, feature height is color-coded using false-coloring. Elevated features are shown in bright colors with depressions in dark colors. Changes in surface topography are evident in the surface after the experimental suite (Fig. 11). The surface roughness and peak-to-valley differential for the fracture surface are 4.1 and 77.9 μm before the experiments and increases to 6.1 and 122.4 μm after. We hypothesize that the smooth surface of the fracture is indented by the proppant that creates small pits. The creation of small pits on surface causes increased surface roughness and peak-to-

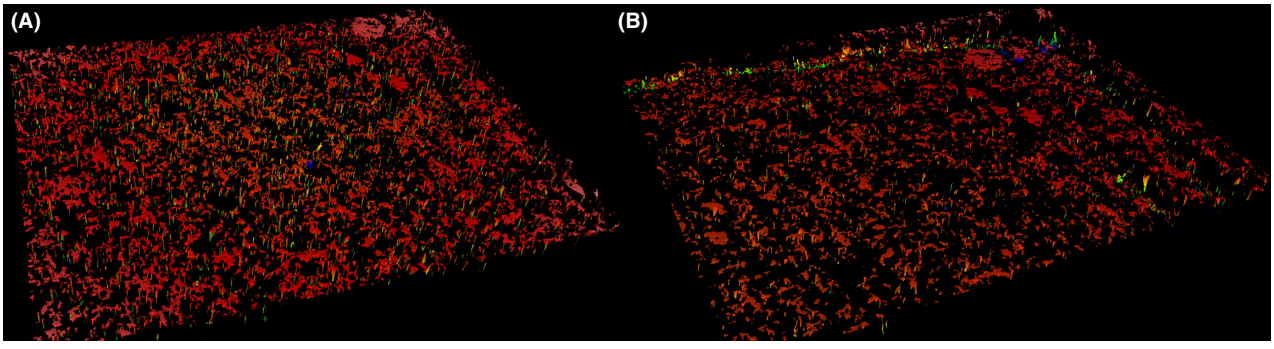

Fig. 11. The aerial view of shale surface (A) before (left) and (B) after (right) the experiment. The features are falsely colored according to their height. The vertical features are highly exaggerated (on the order of several microns). Red represents the highest elevations and blue the depressed features on the surface. The black regions indicate poorly reflecting deep pits with poor signals. The patch shown is 2.3 × 1.7 mm (i.e., the vertical and horizontal scales differ by several orders of magnitude).

valley differential in the measurements. The indentation of proppant in fracture surface reduces the effective fracture aperture and concomitantly reduces the permeability.

CONCLUSIONS

Experimental measurements of permeability evolution are reported for shale cores infiltrated by He and CO_2. The following conclusions are drawn from this study.

(1) The He permeability of shale increases with gas pressure at constant confining stress. The He permeability increases by approximately 15% as the gas pressure is varied from 1 to 6 MPa at a constant confining stress of 10 MPa. The permeability decreases with confining stress (10 MPa >15 MPa >20 MPa).

(2) The adsorption of CO_2 in shale may reduce the permeability by a factor of two. The permeability may reset to the original magnitude if sufficient time is allowed for the sample to release the sorptive gas.

(3) The permeability of shale decreases with gas (CO_2) pressure and the reduction in permeability with gas pressure halts at a critical pressure corresponding to the point at which maximum adsorption is achieved. Beyond this pressure threshold (~double the Langmuir pressure), the permeability increases as a consequence of elevated influence of the diminishing effective stress corresponding to a typical 'U-shaped' form of permeability with gas pressure (Wang *et al.* 2011; Kumar *et al.* 2012).

(4) The He permeability of the propped fracture increases approximately 2- to 3fold that of the nonpropped fracture. The He permeability increases with gas pressure at a constant confining stress. The CO_2 permeability of the propped fracture may decrease by as much as a factor of two as the gas pressure is increased from 1 to 4 MPa at constant confining stress. However, the permeability of the nonpropped fracture increases with gas pressure.

(5) The surface roughness and peak-to-valley differential for the fracture surface are 4.1 and 77.9 μm, respectively, before the experiments and increase to 6.1 and 122.4 μm at the conclusion of the experimental suite, indicating the significant influence of proppant indentation on the fracture surface.

(6) Permeability evolution trends in shale are shown to be comparable with those for other sorbing media – such as coal. Correspondingly, permeability evolution models developed for coal may be utilized to both explain and to quantify permeability evolution in shale. An excellent match exists between experimental data and the model for intact, nonpropped fractured and propped fractured shale cores.

ACKNOWLEDGEMENTS

This work is as a result of partial support from ExxonMobil-URC. Authors do not have any conflict of interest. Authors would like to thank Josh Stapleton at MRI, Penn State University and Amrita Mukherjee at EI, Penn State University for helping us with Optical Profilometry and Proximate analysis, respectively.

REFERENCES

Agbaji A, Lee B (BT), Kumar H, Belvalkar R, Eslambolchi S, Guiadem S, Park S (2009) *Sustainable Development and Design of Marcellus Shale Play in Susquehanna, PA*. Penn State Univeristy, University Park.

Amyx JW, Bass DM, Whiting RL (1960) *Petroleum Reservoir Engineering: Physical Properties*. McGraw-Hill, New York, NY.

Arthur JD, Bohm B, Layne M (2008) Hydraulic Fracturing Considerations for Natural Gas Wells of the Marcellus Shale. *The Ground Water Protection Council*, 2008 Annual Forum Cincinnati, OH.

ASTM International D7582 (2010) *Standard test methods for proximate analysis of coal and coke by macro thermogravimetric analysis*. IHS, West Conshohocken, PA.

Bai M, Roegiers J-C, Elsworth D (1995) Poromechanical response of fractured-porous rock masses. *Journal of Petroleum Science and Engineering*, **13**, 155–168.

van Bergen F, Pagnier H, Krzystolik P (2006) Field experiment of enhanced coalbed methane-CO2 in the upper Silesian basin of Poland. *Environmental Geosciences*, **13**, 201–224.

Bower AF, Fleck NA, Needleman A, Ogbonna N (1993) Indentation of a power law creeping solid. *Proceedings of the Royal Society of London, Series A: Mathematical and Physical Sciences*, **441**, 97–124.

Boyer C, Kieschniek J (2010) Producing gas from its source. In: *Oilfield Review Schlumberger*. Schlumberger, Houston, TX.

Brace WF, Walsh JB, Frangos WT (1968) Permeability of granite under high pressure. *Journal of Geophysical Research*, **73**, 2225–2236.

Bruner KR, Smosna R (2011) A comparative study of the Mississippian Barnett Shale, Fort Worth Basin, and Devonian Marcellus Shale, Appalachian Basin. In: *The Energy Lab Publications* (ed Soeder DJ), pp. 1–106. Pittsburgh, PA, US-DOE.

Bustin RM, Cui X, Chikatamarla L (2008) Impacts of volumetric strain on CO2 sequestration in coals and enhanced CH4 recovery. *AAPG Bulletin*, **92**, 15–29.

Chen G, Chenevert ME, Sharma MM, Yu M (2003) A study of wellbore stability in shales including poroelastic, chemical, and thermal effects. *Journal of Petroleum Science and Engineering*, **38**, 167–176.

Cho Y, Ozkan E, Apaydin OG (2012) Pressure-Dependent Natural-Fracture Permeability in Shale and its Effect on Shale-Gas Well Production. *SPE Annual Technical Conference and Exhibition*. Society of Petroleum Engineers, San Antonio, TX, USA.

Cui X, Bustin RM, Chikatamarla L (2007) Adsorption-induced coal swelling and stress: implications for methane production and acid gas sequestration into coal seams. *Journal of Geophysical Research*, **112**, B10202.

Curtis JB (2002) Fractured shale-gas systems. *AAPG Bulletin*, **86**, 1921–1938.

Day S, Fry R, Sakurovs R, Weir S (2010) Swelling of coals by supercritical gases and its relationship to sorption. *Energy & Fuels*, **24**, 2777–2783.

Dong J-J, Hsu J-Y, Wu W-J, Shimamoto T, Hung J-H, Yeh E-C, Wu Y-H, Sone H (2010) Stress-dependence of the permeability and porosity of sandstone and shale from TCDP Hole-A. *International Journal of Rock Mechanics and Mining Sciences*, **47**, 1141–1157.

Durucan S, Edwards JS (1986) The effects of stress and fracturing on permeability of coal. *Mining Science and Technology*, **3**, 205–216.

Durucan S, Shi J-Q (2009) Improving the CO_2 well injectivity and enhanced coalbed methane production performance in coal seams. *International Journal of Coal Geology*, **77**, 214–221.

Elsworth D, Goodman RE (1986) Characterization of rock fissure hydraulic conductivity using idealized wall roughness profiles. *International Journal of Rock Mechanics and Mining Sciences*, **23**, 233–244.

Elsworth D, Wang S, Izadi G, Kumar H, Mathews J, Liu J, Lee D-S & Pone D (2011) Complex process couplings in systems pushed far-from-equilibrium: Applications to CO_2 sequestration in carboniferous formations. In: *CO_2 Storage in Carboniferous Formations and Abandoned Coal Mines* Vol. 1, (eds He M, Sousa LR, Elsworth D, Vargas E), pp. 55–69. CRC Press, London.

Fathi E, Akkutlu I (2009) Matrix heterogeneity effects on gas transport and adsorption in coalbed and shale gas reservoirs. *Transport in Porous Media*, **80**, 281–304.

Gash BW, Volz RF, Potter G, Corgan JM (1993) In The effect of cleat orientation and confining pressure on cleat porosity, permeability and relative permeability in coal. *International Coalbed Methane Conference*. University of Alabama, Tuscaloosa, Alabama, 247–255.

Harpalani S, Chen G (1995) Estimation of changes in fracture porosity of coal with gas emission. *Fuel*, **74**, 1491–1498.

Harpalani S, Schraufnagel RA (1990) Shrinkage of coal matrix with release of gas and its impact on permeability of coal. *Fuel*, **69**, 551–556.

Jamari J, Schipper DJ (2005) Experimental investigation of fully plastic contact of a sphere against a hard flat. *Journal of Tribology*, **128**, 230–235.

Jenkins CD, Boyer CM II (2008) Coalbed- and shale-gas reservoirs. *SPE Journal of Petroleum Technology*, **60**, 92–99.

Kang SM, Fathi E, Ambrose RJ, Akkutlu IY, Sigal RF (2011) Carbon dioxide storage capacity of organic-rich shales. *SPE Journal*, **16**, 842–855.

Kelemen SR, Kwiatek LM (2009) Physical properties of selected block Argonne Premium bituminous coal related to CO2, CH4, and N2 adsorption. *International Journal of Coal Geology*, **77**, 2–9.

Kiyama T, Nishimoto S, Fujioka M, Xue Z, Ishijima Y, Pan Z, Connell LD (2011) Coal swelling strain and permeability change with injecting liquid/supercritical CO2 and N2 at stress-constrained conditions. *International Journal of Coal Geology*, **85**, 56–64.

Klinkenberg LJ (1941) *The Permeability of Porous Media To Liquids And Gases*. pp. 200–213 American Petroleum Institute, Tulsa, OK.

Kumar H, Pone JDN, Mitchell GD, Halleck PM, Mathews JP (2009) In Lithotype influences on (an idealized) coal cleat surface deformation by carbon dioxide induced coal swelling. *International Coalbed Methane and Oil Shale Symposium*. Tuscaloosa, Alabama.

Kumar H, Elsworth D, Marone CJ, Mathews J (2010) Permeability evolution of shale and coal under differential sorption of He, CH4 and CO2. *American Geophysical Union, Fall Meeting 2010*. San Francisco.

Kumar H, Elsworth D, Liu J, Pone D, Mathews JP (2012) Optimizing enhanced coalbed methane recovery for unhindered production and CO2 injectivity. *International Journal of Greenhouse Gas Control*, **11**, 86–97.

Kumar H, Elsworth D, Liu J, Pone D & Mathews JP (2014) Permeability Evolution of Propped Artificial Fractures in Coal on Injection of CO_2. *Journal of Petroleum Science and Engineering* (Submitted).

Kumar H, Elsworth D, Mathews JP, Liu J, Pone D (2014) Effect of CO2 injection on heterogeneously permeable coalbed reservoirs. *Fuel*, **135**, 509–521.

Laubach SE, Marrett RA, Olson JE, Scott AR (1998) Characteristics and origins of coal cleat: a review. *International Journal of Coal Geology*, **35**, 175–207.

Letham EA (2011) Matrix permeability measurements of gas shales: gas slippage and adsorption as sources of systematic error. In: *Geological Science Vancouver*. The University of British Columbia, Vancouver.

Liu J, Elsworth D, Brady BH (1997) Analytical evaluation of post-excavation hydraulic conductivity field around a tunnel. *International Journal of Rock Mechanics and Mining Sciences*, **34**,181.e181–181.e187.

Liu J, Wang J, Chen Z, Wang S, Elsworth D, Jiang Y (2011) Impact of transition from local swelling to macro swelling on the evolution of coal permeability. *International Journal of Coal Geology*, **88**, 31–40.

Loucks RG, Reed RM, Ruppel SC, Jarvie DM (2009) Morphology, genesis and distribution of nanometer-scale pores in Siliceous mudstones of the Mississippian Barnett shale. *Journal of Sedimentary Research*, **79**, 848–861.

Mastalerz M, He L, Melnichenko YB, Rupp JA (2012) Porosity of coal and shale: insights from gas adsorption and SANS/USANS techniques. *Energy & Fuels*, **26**, 5109–5120.

Mesarovic SD, Fleck NA (2000) Frictionless indentation of dissimilar elastic–plastic spheres. *International Journal of Solids and Structures*, **37**, 7071–7091.

Min K-B, Rutqvist J, Elsworth D (2009) Chemically and mechanically mediated influences on the transport and mechanical characteristics of rock fractures. *International Journal of Rock Mechanics and Mining Sciences*, **46**, 80–89.

Nuttall BC (2010) Reassessment of CO2 sequestration capacity and enhanced gas recovery potential of middle and upper Devonian black shales in the Appalachian Basin. *MRCSP Phase II Topical Report*. Kentucky Geological Survey, Lexington, Kentucky, 1–48.

Nuttall BC, Eble CF, Drahovzal JA, Bustin AMM (2005) *Analysis of Devonian Black Shales in Kentucky for Potential Carbon Dioxide Sequestration and Enhanced Natural Gas Production*. Kentucky Geological Survey, Lexington, Kentucky.

Palmer I (2009) Permeability changes in coal: analytical modeling. *International Journal of Coal Geology*, **77**, 119–126.

Pellenq RJ-M, Brochard L, Damme MV, Ulm F-J (2012) *From the Fundamentals of Porous Carbons Poromechanics to Applications for CO2 Sequestration and Gas-Shale*. AIChE Pittsburgh, Pittsburgh, PA.

Perez E, Kaproth BM, Haines S, Saffer D (2010) Laboratory measurements of permeability reduction in naturally occurring shear bands formed in unlithified sands. *106th Annual Meeting, and Pacific Section, American Association of Petroleum Geologists*. Geological Society of America, Anaheim, CA 42, 84.

Piggott AR, Elsworth D (1993) Laboratory assessment of the equivalent apertures of a rock fracture. *Geophysical Research Letters*, **20**, 1387–1390.

Pini R, Ottiger S, Burlini L, Storti G, Mazzotti M (2009) Role of adsorption and swelling on the dynamics of gas injection in coal. *Journal of Geophysical Research*, **114**, B04203.

Pone JDN, Halleck PM, Mathews JP (2010) 3D characterization of coal strains induced by compression, carbon dioxide sorption, and desorption at in-situ stress conditions. *International Journal of Coal Geology*, **82**, 262–268.

Rahmanian MR, Solano N, Aguilera R (2010) Storage and output flow from shale and tight gas reservoirs. *SPE Western Regional Meeting*. Society of Petroleum Engineers, Anaheim, CA, USA.

Reucroft PJ, Patel H (1986) Gas-induced swelling in coal. *Fuel*, **65**, 816–820.

Rousseau D, Sonwai S, Khan R (2010) Microscale surface roughening of chocolate viewed with optical profilometry. *Journal of the American Oil Chemists' Society*, **87**, 1127–1136.

Sakhaee-Pour A, Bryant S (2012) Gas permeability of shale. *SPE Reservoir Evaluation & Engineering*, **15**, 401–409.

Seidle JR, Huitt LG (1995) Experimental measurement of coal matrix shrinkage due to gas desorption and implications for cleat permeability increases. *International Meeting on Petroleum Engineering*, Society of Petroleum Engineer.

Seidle JP, Jeansonne MW, Erickson DJ (1992) Application of matchstick geometry to stress dependent permeability in coals. *SPE Rocky Mountain Regional Meeting*. SPE, Casper, Wyoming.

Shi J-Q, Durucan S (2010) Exponential growth in San Juan Basin Fruitland coalbed permeability with reservoir drawdown: model match and new insights. *SPE Reservoir Evaluation & Engineering*, **13**, 914–925.

Siemons N, Busch A (2007) Measurement and interpretation of supercritical CO2 sorption on various coals. *International Journal of Coal Geology*, **69**, 229–242.

Soeder DJ (1988) Porosity and permeability of eastern Devonian gas shale. *SPE Formation Evaluation*, **3**, 116–124.

Somerton WH, Söylemezoglu IM, Dudley RC (1975) Effect of stress on permeability of coal. *International Journal of Rock Mechanics and Mining Sciences & Geomechanics Abstracts*, **12**, 129–145.

Veatch RWJ, Moschovidis ZA, Fast CR (1989) *An Overview of Hydraulic Fracturing-Recent Advances in Hydraulic Fracturing*, Society of Petroleum Engineers, Richardson, TX.

Wang FP, Reed RM (2009) Pore networks and fluid flow in gas shales. *SPE Annual Technical Conference and Exhibition* New Orleans, Louisiana, Society of Petroleum Engineers.

Wang S, Elsworth D, Liu J (2011) Permeability evolution in fractured coal: the roles of fracture geometry and water content. *International Journal of Coal Geology*, **87**, 13–25.

Wang S, Elsworth D, Liu J (2012) A mechanistic model for permeability evolution in fractured sorbing media. *Journal of Geophysical Research*, **117**, B06205.

White CM, Smith DH, Jones KL, Goodman AL, Jikich SA, LaCount RB, DuBose SB, Ozdemir E, Morsi BI, Schroeder KT (2005) Sequestration of carbon dioxide in coal with enhanced coalbed methane recovery-a review. *Energy & Fuels*, **19**, 659–724.

Zhu WC, Liu J, Sheng JC, Elsworth D (2007) Analysis of coupled gas flow and deformation process with desorption and Klinkenberg effects in coal seams. *International Journal of Rock Mechanics and Mining Sciences*, **44**, 971–980.

SUPPORTING INFORMATION

Additional Supporting Information may be found in the online version of this article:

Figure S1. Rawdata Figure S1.

Figure S2. Rawdata Figure S2.

Figure S3. Rawdata Figure S3.